

Article

Gemological Characteristics and Chemical Composition of a New Type of Black Jadeite and Three Imitations

Beiqi Zheng ^{1,2} , Ke Li ^{3,*} and Yuyang Zhang ⁴ ¹ School of Environment, Harbin Institute of Technology, Harbin 150090, China; 11849578@mail.sustech.edu.cn² Department of Earth and Space Sciences, Southern University of Science and Technology, Shenzhen 518055, China³ Institute of Technical Information for Building Materials Industry, Beijing 100024, China⁴ Gemmological Institute, China University of Geosciences, Wuhan 430074, China; gembubble@cug.edu.cn

* Correspondence: 18820691757@163.com

Abstract: Because of the increasing price of jadeite, many fake species have appeared on the market. We recognized three pieces of fake black jadeite that had been placed among real black jadeite. In this study we conducted a mineralogical investigation of the three fakes and the real jadeite by using FTIR and XRD techniques; in addition, we performed in situ major, minor and trace element chemical characterization based on EPMA-WDS and LA-ICP-MS techniques. The three imitations have different components, dominated by katophorite (97%), augite (66%) and anorthite (97%). In contrast, the real jadeite sample contains more than 99% jadeite. Unlike previous reports on black jadeite, the dark omphacite exsolution around the jadeite cleavage is the chromogenic factor in the present study, whereas the black color of the imitations comes from light absorption by major melanocratic minerals and widespread fine graphite. We propose that 2–4 sharp bands between 600 and 800 cm⁻¹ of FTIR and the 2.42 and 2.49 Å peaks of XRD can be used to discriminate black jadeite from imitations. Even though natural jadeite deposits are being exhausted, materials of the three natural imitations were determined not to be suitable for jewelry due to low hardness, widespread occurrence and unknown injury of the radioactive elements thorium and uranium. Otherwise, they could enhance value and be ideal for large-sized ornaments of fine design.

Keywords: jadeite; composition; colorization mechanism; imitation



Citation: Zheng, B.; Li, K.; Zhang, Y. Gemological Characteristics and Chemical Composition of a New Type of Black Jadeite and Three Imitations. *Crystals* **2022**, *12*, 658. <https://doi.org/10.3390/cryst12050658>

Academic Editors: Taijin Lu, Fei Liu, Tingting Gu and Francesco Capitelli

Received: 28 February 2022

Accepted: 29 April 2022

Published: 4 May 2022

Publisher's Note: MDPI stays neutral with regard to jurisdictional claims in published maps and institutional affiliations.



Copyright: © 2022 by the authors. Licensee MDPI, Basel, Switzerland. This article is an open access article distributed under the terms and conditions of the Creative Commons Attribution (CC BY) license (<https://creativecommons.org/licenses/by/4.0/>).

1. Introduction

Jadeite, also called “Feicui” or Myanmar jade, is generally accepted as the king of jades. The national standard of China defines it as containing mostly jadeite, or it includes a rare Na–Ca-rich pyroxene group mineral such as omphacite or sodium chromium pyroxene. To date, there is still no boundary line where the content of jadeite reaches a level to be defined as Feicui [1].

Earlier, Yin (1990) proposed that Feicui should have more than 90% jadeite [2], but synchronous research showed that Feicui originating from Myanmar [3] contained more than 10% omphacite. Therefore a “diopside-type” standard was proposed that comprised both diopside and jadeite. Later, Zou suggested a limit of 50% jadeite for Feicui [4].

Because Myanmar’s jadeite deposits are being exhausted and its political scene is turbulent, the market price for jadeite shows a continuous spike. Black jadeite used to be valueless, but in recent years, up-market black jadeite has attracted more and more consumers [5]. However, non-transparent black jadeite and its imitations usually have a more complex composition, so conventional analysis cannot make fine distinctions. Therefore, aside from traditional fake jadeite (so-called B jade and C jade), separate associated minerals such as sodium feldspathic jade [6] have been reported as imitations. However, the highly similar characteristic of such natural imitation jadeite is easily confused. The lack of uniform standards leads to different definitions for one sample. As a result, the testing

center usually returns such samples to the consumer instead of providing an accurate name. The samples in this study were derived from a batch of black jadeite, and after detailed discrimination we found three of them to be fake. We conducted in situ major, minor, trace element and XRD analyses to: (1) explore their colorization mechanism; (2) confirm phase components and provide diagnostic proof; (3) reevaluate whether such natural imitations have the potential to be made into jewelry.

2. Sample Description

This study focuses on four samples, all of which were made into pendants by fine engraving. They are black in both reflected and transmission light, non-transparent, medium-to-fine grained and with vitreous luster. The four samples has high thermal conductivity and thus it feels cold. Hand specimens are recognized as polycrystalline aggregates and exhibit weak cleavage, but glistening is locally visible in each sample, indicating a common development of cleavage. After we cut them into thin pieces, each sample exhibited a different phenomenon through light: part of Sample 1 was aquamarine blue while the other part was yellow (Figure 1b); Sample 2 was yellow-green to green (Figure 1d); Sample 3 and Sample 4 were both composed of a colorless background and a mass of crumby or punctate black minerals (Figure 1f,h).

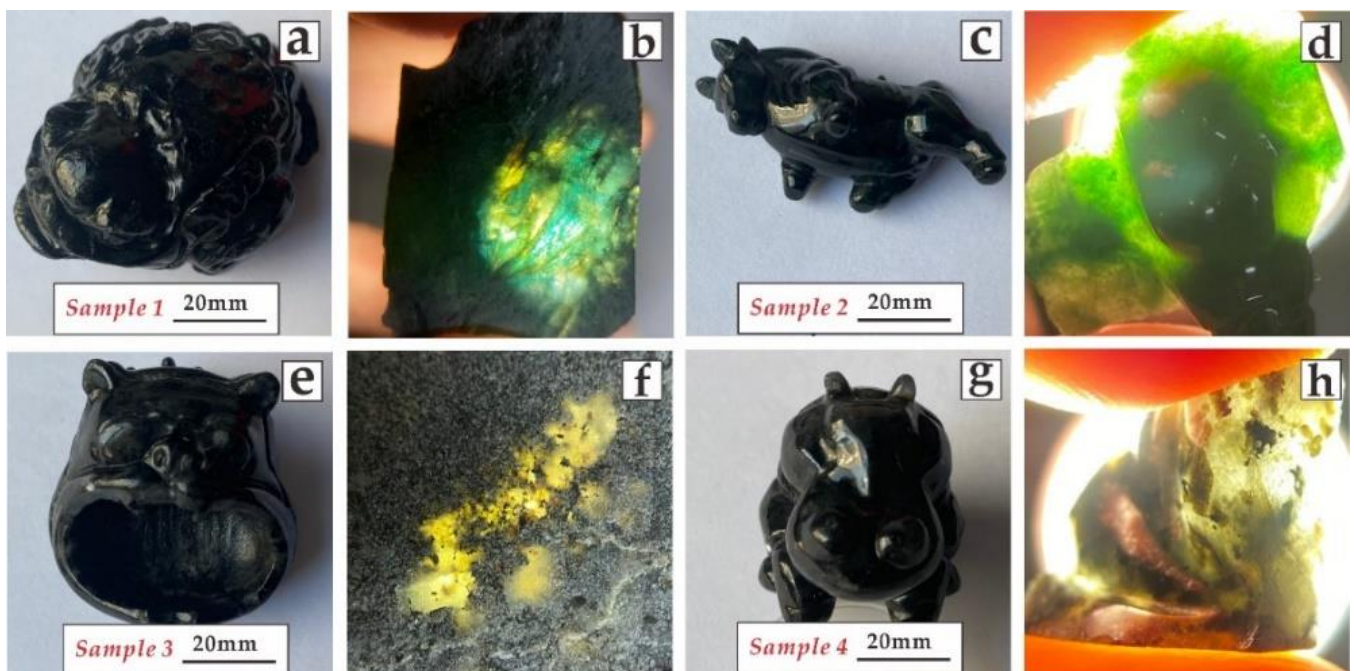


Figure 1. Photograph and corresponding light transmission images of the four samples:(a) Sample 1 shows worst polishing status; (b) aquamarine blue and yellow are both showed in Sample 1; (c) Sample 2 shows the homogenous appearance; (d) homogenous color distribution of yellow-green to green in Sample 2; (e) fine engraving of Sample 3; (f) unknown crumby or punctate black minerals in Sample 3; (g) white “snowflake floc” are widespread on Sample 4; (h) unknown black minerals but chiefly as crumby appearance present in Sample 4.

In all the samples, the so-called orange-peel phenomenon was observed, but Sample 1 showed the worst polishing status, probably due to weaker rigidity. White “snowflake floc” was present in Samples 1, 3 and 4, while Sample 2 was homogenous (Figure 1a,c,e,g).

Each sample was distinct under the microscope: the dominant mineral of Sample 1 was colorless to light pink with perfect cleavage in one direction (Figure 1a,b)

Sample 2 was composed of almost a single mineral: colorless through plane-polarized light but grey-to-dark grey under cross-polarized light and showing a fine grain with fine

cleavage in one direction. Black matter filled in the cleavage and the sample developed typical granoblastic texture.

Sample 3 contained at least three major minerals: feldspar developed typical polysynthetic twinning and medium-perfect cleavage in two directions. One other mineral was distinguished by its cleavage angle of nearly 90° . The other mineral was distinguished by advanced white interference and developed rhombohedral cleavage in three directions. Sample 4 was dominated by feldspar, but we found another mineral that was also present in Sample 3 that had a dominant white interference color and rhomboid cleavage. One kind of unknown mineral common to these two samples was black and exists in the forming of grain filling or a single euhedral grain.

3. Methods

Regular analysis—non-destructive testing of density and refractive index as well as destructive testing of hardness—was conducted on these four samples, after which they were pretreated into microprobe slices and powdered for subsequent analysis.

3.1. Sample Composition

The present study consisted of both quantitative and semi-quantitative analyses for mineral characterization. We used infrared spectra to qualitatively analyze mineral species and X-ray diffraction (XRD) to determine phase composition, while EPMA and LA-ICP-MS were used to measure the major, minor and trace element composition in a thin section.

Infrared spectra analysis was performed by using a Bruker Vertex 80 Fourier-transform infrared (FTIR) spectrometer from Gemmological Institute, China University of Geosciences, Wuhan. The reflection method was operated under the following conditions: 64 scans, $400\text{--}2000\text{ cm}^{-1}$ range, and 4 cm^{-1} resolution. This analysis was based on nondestructive specular reflection. The result in Figure 2 was processed by a Kramers–Kronig transformation.

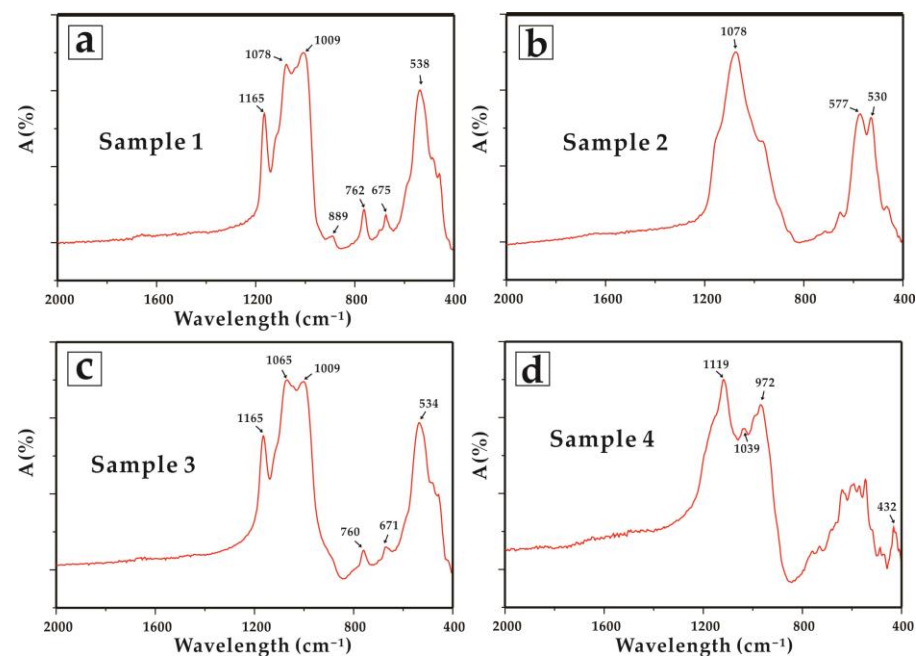


Figure 2. Infrared spectra after K–K transformation: (a) Sample 1; (b) Sample 2; (c) Sample 3; (d) Sample 4.

XRD data were collected using a Dmax2600 from CTC Beijing Testing Technology Service Co., Ltd., Beijing, China. We used 40 kV, 150 mA, and Cu $K\alpha$ radiation of wavelengths $K\alpha_1 = 1.5406\text{ \AA}$ and $K\alpha_2 = 1.54439\text{ \AA}$, and a $K\alpha_1/K\alpha_2$ ratio of 0.3. Diffractograms were recorded from $10\text{--}80^\circ 2\theta$, in $0.021^\circ 2\theta$ increments with a 1.0 s counting time per increment.

The total analysis time was 66 min. The semi-quantitative XRD method was based on X-ray powder diffraction and the minerals from the ICDD database that were used in the Bruker EVA[®] Software. The first step was mineral identification, and then the peaks of each mineral were manually scaled to give the best fit for the observed XRD diffractogram. The minerals used for the mineral quantification in this study were ordered microcline (Mc) with triclinic structure, ordered albite (Ab) with low temperature with triclinic structure and synthetic quartz (Qtz) with trigonal structure.

The semi-quantitative mineralogy based on 2 θ -intensity data analyzed by the XRD instrument was further used in Topas Rietveld software for XRD structural refinement. The structural refinement considered parameters such as peak shape, peak width and preferred orientation, and it enabled the modelling of the broad anisotropic peak. Anisotropic peak broadening was included to account for the complex peak-broadening observed in the feldspars. The broadening was caused by small variations in the chemical composition of the feldspar and by the several symmetry changes after being subjected to cooling. The anisotropic peak broadening took into account the effects of both solid-solution and symmetry changes.

3.2. Chemical Analysis

Mineral compositions were analyzed with a JEOL JXA-8230 Electron Probe Microanalyzer equipped with five wavelength-dispersive spectrometers (WDS) at the Laboratory of Microscopy and Microanalysis, Wuhan Microbeam Analysis Technology Co., Ltd. Details of analytical procedures are described in Yang et al. (2022) [7]. The samples were first coated with a thin conductive carbon film prior to analysis. The precautions suggested by Zhang and Yang (2016) [8] were used to minimize the difference of carbon film thickness between samples to obtain a uniform ca. 20 nm coating. Operating conditions for quantitative WDS analyses involved an accelerating voltage of 15 kV, a beam current of 20 nA and a 10 μ m spot size. Data were corrected online using a ZAF (atomic number, absorption, fluorescence) correction procedure. The peak counting time was 10 s for Ca, Mg, K, F, Si, Al, Fe, Na, Ti, and Mn. The background counting time was 1/2 of the peak counting time on the high- and low-energy background positions. The following standards were used: Diopside (Ca, Mg), Sanidine (K), Barium Fluoride (F), Olivine (Si), Pyrope Garnet (Fe, Al), Jadeite (Na), Rutile (Ti), Rhodonite (Mn). The major elements of the minerals are listed in Tables 1 and 2. The mapping of Al, Fe, Mg, Ca and Na on Sample 2 was conducted using an Oxford AZtecLive UltimMax 100 EDX spectroscope equipped with electron microprobe analysis (EMPA).

Table 1. Major element compositions of katophorite, omphacite and jadeite in Samples 1 and 2.

Spot	Sample 1					Sample 2											
	1	2	3	4	5	1	2	3	4	5	6	7	1	2	3	4	
Type	Katophorite					Omphacite					Jadeite						
SiO ₂	54.54	55.08	57.30	56.96	59.40	57.36	56.49	57.35	55.86	56.34	55.78	56.23	59.17	59.94	59.22	59.26	
TiO ₂	0.08	0.06	0.02	0.04	0.03	0.07	0.09	0.14	0.22	0.20	0.08	0.08	0.29	0.27	0.05	0.11	
Al ₂ O ₃	9.08	6.78	5.97	7.21	5.04	10.67	10.71	14.91	10.38	14.25	11.85	11.32	22.13	22.73	21.64	22.41	
FeO	5.67	4.77	4.01	4.21	4.04	2.91	3.89	3.96	5.69	4.67	4.87	4.73	1.45	1.32	1.82	1.79	
MnO	0.10	0.08	0.10	0.14	0.13	0.10	0.11	0.13	0.11	0.13	0.20	0.16	0.01	0.00	0.08	0.02	
MgO	15.08	17.13	17.13	16.11	17.67	8.17	7.88	5.66	7.67	6.39	7.51	7.63	1.45	1.31	1.72	1.53	
CaO	1.67	2.55	1.26	1.01	1.46	12.85	12.26	8.57	11.11	8.74	12.62	12.82	2.10	1.76	2.71	2.20	
Na ₂ O	8.85	8.61	9.32	9.43	8.01	6.66	6.87	9.75	7.24	8.93	7.12	7.21	12.62	12.07	12.24	13.56	
K ₂ O	0.24	0.25	0.32	0.17	0.35	0.00	0.01	0.00	0.04	0.01	0.00	0.01	0.00	0.02	0.00	0.00	
Total	95.31	95.30	95.43	95.27	96.12	98.79	98.31	100.46	98.31	99.64	100.02	100.18	99.22	99.43	99.48	100.88	

Table 2. Major element compositions of katophorite, amphibole and jadeite in Samples 3 and 4.

Number	Sample 3			Sample 4			Sample 3			Sample 4		
	Spot	1	2	3	1	2	3	1	2	3	1	2
Type	Augite						Anorthite					
SiO ₂	52.88	51.98	52.98	52.21	52.23	51.96	46.50	46.54	43.77	45.90	44.49	44.13
TiO ₂	0.18	0.20	0.20	0.20	0.22	0.18	0.03	0.02	0.01	0.01	0.02	0.00
Al ₂ O ₃	1.06	1.30	1.14	1.06	1.06	1.24	33.56	33.38	35.62	33.64	34.60	34.95
FeO	20.01	20.13	20.08	20.51	19.57	19.76	0.45	0.40	0.44	0.60	0.30	0.28
MnO	0.68	0.64	0.70	0.70	0.73	0.69	0.02	0.02	0.01	0.01	0.00	0.00
MgO	23.21	23.19	23.62	23.14	23.39	23.04	0.05	0.06	0.02	0.18	0.01	0.00
CaO	1.49	1.61	1.05	1.17	1.76	1.35	17.02	16.70	19.14	17.35	18.38	18.66
Na ₂ O	0.00	0.00	0.02	0.01	0.02	0.01	1.38	1.65	0.49	1.22	0.75	0.60
K ₂ O	0.00	0.01	0.00	0.00	0.00	0.00	0.02	0.01	0.00	0.01	0.00	0.00
Total	99.51	99.06	99.80	99.00	98.98	98.22	99.02	98.77	99.50	98.91	98.54	98.63
An							87.21	84.81	95.61	88.69	93.11	94.47

Analyses of minerals in thin sections were conducted by the LA-ICP-MS method at the Wuhan SampleSolution Analytical Technology Co., Ltd., Wuhan, China. The testing points followed a straight line from the dark to the light part. A photon machine analyte HE-193-nm ArF excimer laser ablation system and Agilent 7900 quadrupole ICP-MS were combined for the experiments. This laser ablation system comprised a squid signal smoothing device. The 193 nm ArF excimer laser, homogenized by a set of beam delivery systems, was focused on a mineral surface with a fluent of approximately 2 J/cm². The ablation protocol employed a spot diameter of 35 µm at an 8 Hz repetition rate for 40 s after measuring the gas blank for 20 s. Helium was applied as the carrier gas to transport aerosols to ICP-MS efficiently. Standard reference materials, including GCS-1G, BCR-2G and GSE-1G, and NIST 612, were used as external calibration standards. Standard reference materials were run after every 6–8 testing points; a calculation was conducted for every element in every plot analysis.

Raw data reduction was performed offline by ICPMSDataCal software without applying internal standardization [9]. Each spectrum was carefully examined. Segments of the spectrum related to mineral inclusions were removed. Measured values of these reference glasses that deviated from preferred values were typically better than ±5% for major elements and ±10% for trace elements. The trace elements of the tourmalines are listed in Table S1 (see Supplementary Materials).

4. Results

Regular analysis shows distinct Moh's hardness in these four samples: 5 for Sample 1, 6.5 for Sample 2, and 6 for Sample 3 and Sample 4. Sample 1 to Sample 4 exhibited a density of 3.26 g/cm³, 3.33 g/cm³, 3.45 g/cm³ and 2.75 g/cm³, respectively. Samples 1, 2 and 3 had the same refractive index (1.66) while Sample 4 had a lower value of 1.54.

FTIR diffuse reflectance spectra were collected in the low-frequency region of 400–2000 cm⁻¹ (Figure 2a–d). Different patterns of infrared spectra can be seen in the four samples. Patterns of Sample 1 and Sample 3 were relatively similar with band at 1165 cm⁻¹, 1009–1070 cm⁻¹, around at 760 cm⁻¹, 670 cm⁻¹ and 535 cm⁻¹. This indicates they mostly conform to amphibole group. But there was no reported atlas that was completely consistent with Sample 1. Sample 2 was identical in most respects to jadeite according to diagnostic 2–4 sharp bands in the range of 600–800 cm⁻¹, whereas Sample 4 was characterized by the most intense peaks band in the range of 950–1200 cm⁻¹ and in agreement with feldspar group but with small intrusively peak caused by other minerals.

XRD analysis shows completely different X-ray powder diffraction patterns: the main peaks of Sample 1 were 8.48, 3.37, 2.70 and 1.78 Å, while those of Sample 2 were 6.22, 4.30, 2.92, 2.49 and 2.42 Å. The main peaks of Sample 3 were 3.17, 2.88, 2.52 Å and those of Sample 4 were 8.40, 3.18, 2.95, 1.79 Å. After calculation, we found distinct mineral assemblage in

these four samples. Sample 1 comprised major katophorite (97%) and minor dolomite (3%), while Sample 3 comprised augite (66%), anorthite (29%) and dolomite (5%), respectively (Figure 3a,c). Sample 4 was dominated by anorthite of nearly 97% with accessory minerals of dolomite (2%) and hornblende (1%) (Figure 3d). Oppositely, Sample 2, which was the real jadeite sample, comprised more than 99% jadeite (Figure 3b).

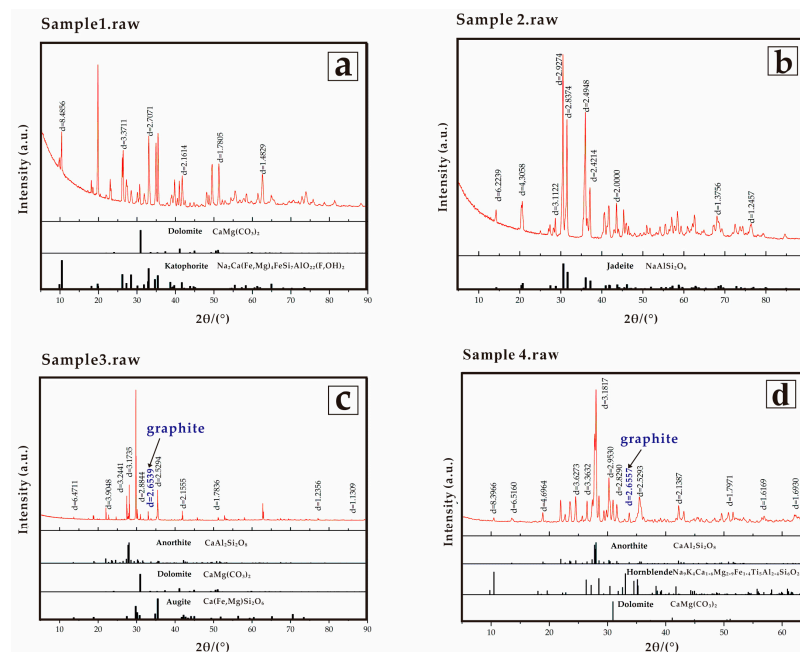


Figure 3. X-ray powder diffraction patterns of (a) Sample 1; (b) Sample 2; (c) Sample 3 and (d) Sample 4.

According to EMPA analysis data, the katophorite of Sample 1 showed wide compositional variations in SiO_2 (54.54–59.40 wt%), TiO_2 (0.02–0.08 wt%), Al_2O_3 (5.04–9.08 wt%), FeO (4.01–5.57 wt%), MnO (0.08–0.14 wt%), MgO (15.08–17.67 wt%), CaO (1.01–2.55 wt%), Na_2O (8.01–9.43 wt%) and K_2O (0.17–0.35 wt%). Minor amounts of augite in Sample 4 could not be identified by XRD. The augites of Samples 3 and 4 exhibited similar major element compositions, for which the difference value of the average contents was within 1% (Figure 4a–g). However, the anorthite of the samples had a wider range of Al_2O_3 , CaO and Na_2O (Figure 4a–c). Unlike anorthite, the major components of augite in these two samples were nearly consistent (Figure 4d–g). The vast majority of Sample 2 was jadeite, and the small differences are shown in the testing points: SiO_2 (59.17–59.94 wt%), TiO_2 (0.05–0.29 wt%), Al_2O_3 (21.64–22.73 wt%), FeO (1.32–1.82 wt%), MnO (0–0.08 wt%), MgO (1.31–1.72 wt%), CaO (1.76–2.71 wt%), Na_2O (12.07–13.56 wt%) and K_2O (0–0.02 wt%). In this sample, we also found a very low percentage of omphacite, which was distinguished by significantly higher CaO (8.57–12.85 wt%) and MgO (5.66–8.17 wt%) but lower Na_2O (6.66–9.75 wt%) and Al_2O_3 (10.38–14.91 wt%) than the jadeite.

More than 40 trace elements were analyzed for these four samples, and the results are more complex than for the major elements. Most had concentrations lower than 10 ppm with higher concentrations observed for Li in the katophorite of Sample 1 (200.4–1115.13 ppm) and the jadeite of Sample 2 (31.60–81.45 ppm). Relatively high V contents were found in augite (95.92–277.26 ppm) but one point of katophorite showed a high content of 134.39 ppm. All samples had low rare earth element (REE) concentrations (the average of sum REE is 4.77 ppm), but comparatively higher Eu content was observed for augite (0–0.69 ppm) and anorthite (0.06–0.43 ppm), but with a slight difference between Sample 3 and Sample 4 (Figure 5e,j). Furthermore, we compared the elements and found markedly higher Cr, Ba and Eu in the anorthite of Sample 4, but the average values of Sr and Zn were very close (Figure 5a–e). Sample 3 exhibited a broader range. However, such

elements, except Cr, were very similar in augite (Figure 5f–j). Radioactive elements were low in all samples except for katophorite in Sample 1 (Th up to 0.84 ppm and U up to 0.06 ppm).

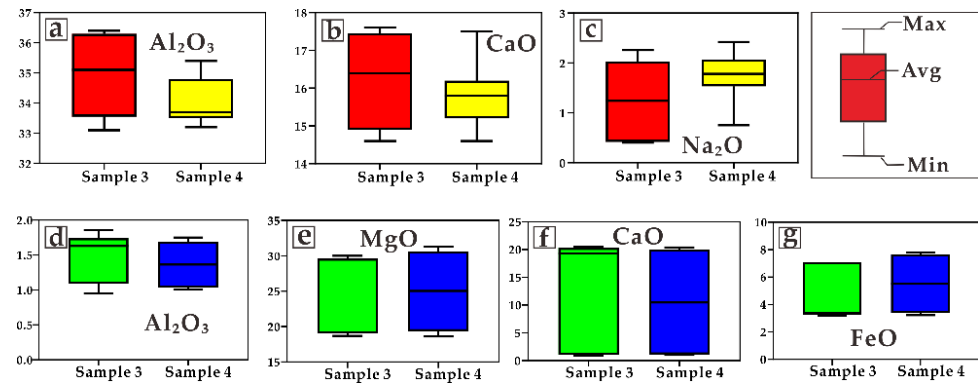


Figure 4. (a–c) Shows major element variations of anorthite and (d–g) shows major element variations of augite between Sample 3 and Sample 4.

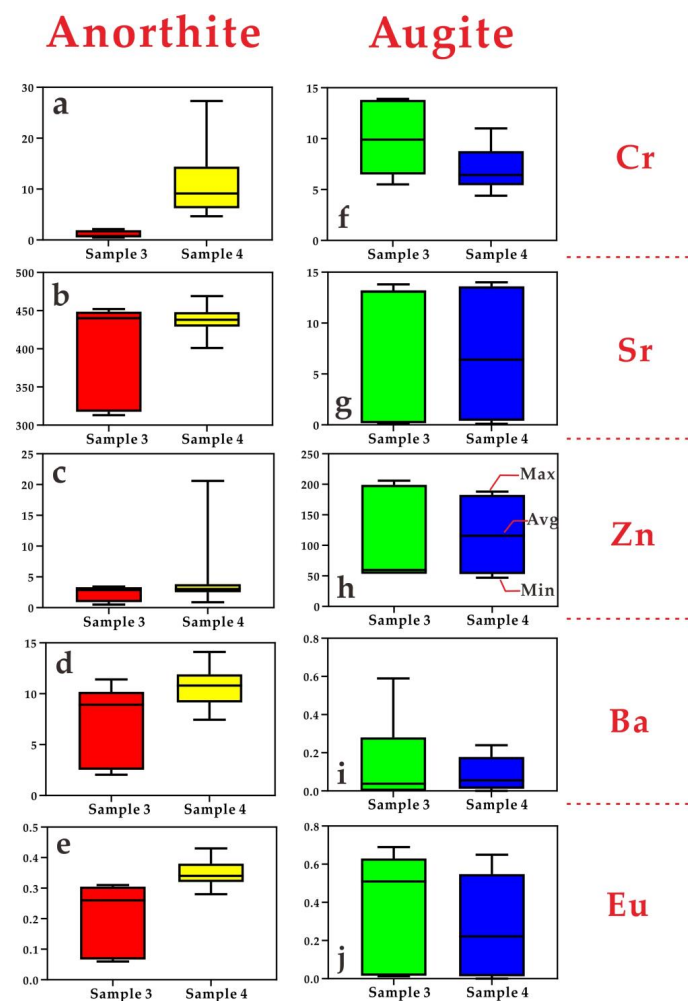


Figure 5. Comparison of the specific trace element variations in anorthite (a–e) and augite (f–j).

5. Discussion

5.1. Chromogenic Factor of Jadeite and Classification of Its Imitations

Black jadeite jade has attracted numerous studies that cover its classification and characteristics. At first, “black-chicken” jadeite was discovered as a mix of 95% jadeite and 5% other minerals or black impurities [10]. Then Yan et al. (2009) [11] divided black jadeite into jadeite and omphacite types, the former being black-chicken jadeite while the latter is “ink” jadeite. The colorization mechanism of black jadeite remains equivocal: (1) dispersion of melanocratic inclusion [10]; (2) black filiform object fracture-filling in jadeite grains [12]; (3) graphite, zircon and ferric oxide that lead to extreme light scattering loss resulting in a large transparency loss [13]; and (4) multiple amorphous carbons directly cause the black color [14,15]. The abovementioned research mostly agrees that the black color is caused by other materials rather than jadeite itself; however, they differ on the type of material and whether it is homochromous.

After careful observation with a polarized microscope, we found no carbon in black jadeite, which matched the analysis data of XRD: no main peak around 2.65 Å (Figure 3b). Moreover, it was distinguishable from jadeite crystallized from the Damukan, Longke or Hpakan deposits because of notably higher Mg and Fe content [16]. As no relationship between Fe and black color has been documented, the black color of jadeite is not caused by its transition elements. Surprisingly, we found dark schlieren crystallized around the jadeite cleavage but has completely different component (Figures 6a–g and 7b). We conducted a detailed EPMA analyses on jadeite and its fracture-filling mineral (Figure 6a). The results (Table 1) show an omphacite component of stoichiometric formula of $(\text{Na}_{0.61}\text{Ca}_{0.36})(\text{Mg}_{0.32}\text{Fe}_{0.13}\text{Al}_{0.59})[\text{Si}_2\text{O}_6]$. This cleavage-filling omphacite exhibited a similar morphology, which supports magmatic genesis that formed after the jadeite [17]. In summary, we suggest that the colorization of black jadeite is due to the exsolution omphacite. We also suggest the jadeite in this study is a new type of black jadeite.

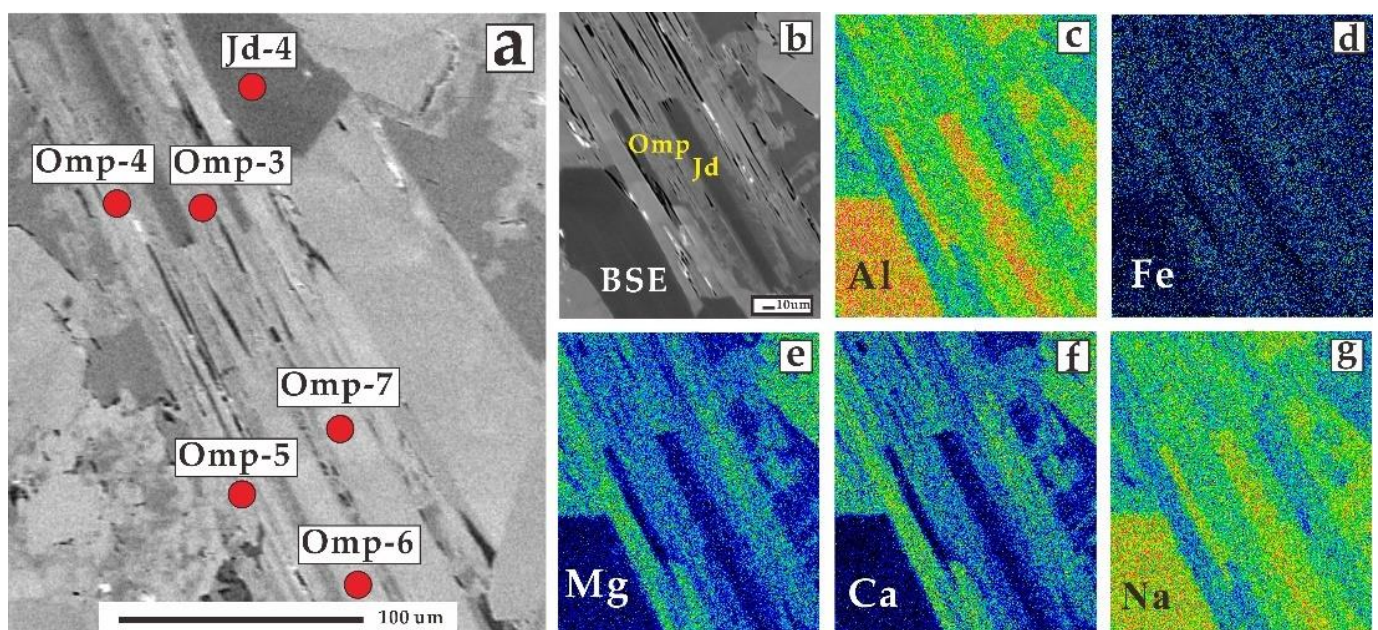


Figure 6. (a) BSE image of the testing positions of jadeite and omphacite exsolution corresponding to Table 1; (b–g) EDX mapping analysis showing major element composition variations among them.

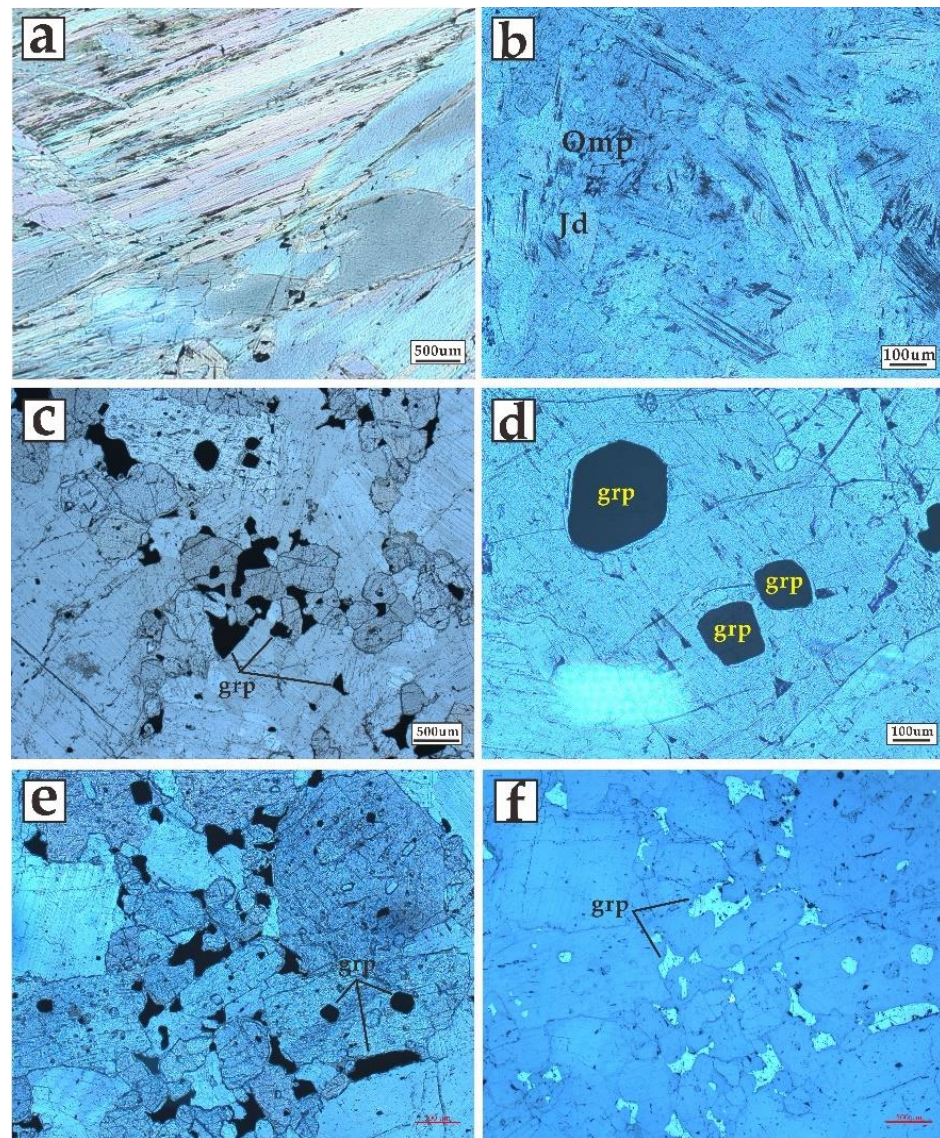


Figure 7. Micrograph of (a) orientation arrangement of katophorite and mica; (b) omphacite schlieren fills in the cleavage of jadeite; (c,d) amorphous and euhedral graphite of Sample 3; (e) dispersed graphite of Sample 4; (f) graphite with metal luster under reflected light.

Sample 3 and 4 in the present study were all considered accessory minerals of Myanmar jadeite [18]. But the sample 1 contains mostly katophorite which is very rare in jadeite. In this sample, minor fine-grained mica showed directional arrangement, indicating that it had suffered from strong metamorphism (Figure 7a). However, the ideal formula for katophorite is $\text{NaCaNaFe}^{2+}_4(\text{AlFe}^{3+})[(\text{Si}_7\text{Al})\text{O}_{22}](\text{OH})_2$ according to Liu et al. (2015) [19]. The considerable Mg content (up to 17.67 wt% in testing points, Table 1), suggests further classification into magnesiokatophorite. Feldspars were present in both Sample 3 and Sample 4, and major element calculation showed that they belong to plagioclase and fall into the bytownite-anorthite solid-solution series, with An 84.81–95.61 for Sample 3 and An 88.69–94.47 for Sample 4, which matches well with the XRD result. The higher Eu contents observed in augite and anorthite are best interpreted as a common substitution of Eu^{2+} for Ca^{2+} [20], and both have a high Ca content. The hornblende group of another study was recognized as an accessory material, or Tinea, on the weathered crust of Feicui, but unlike the blocky appearance in the study, the group commonly has a veinous, disseminated or dendritic structure [21]. Anorthite, the chief component of Sample 4 and main component

of Sample 3, commonly has a white-to-light-grey appearance, and thus these two samples have colorless background. In addition, comparisons in Chapter 4 indicated that no specific element of anorthite can cause the black color (Figure 4a–c; Figure 5a–e). Herein, we cut it into thin sections and found that the black color was due to black mineral inclusions (Figure 1f,h), some of which were documented as melanocratic augite and hornblende (Figure 3c,d). At the same time, we found some other mineral widespread and dispersed with a hexagonal cross-section. They were black under both plane-polarized and cross-polarized light but showed metallic luster under reflected light (Figure 7c–f). In addition, slight 2.65 Å peaks of graphite occurred in both Sample 3 and Sample 4 [15] (Figure 3c,d). We suggest that the material is punctate-euhedral or amorphous graphite because it can absorb incident light on the interior of its host mineral [15]. Therefore, the separate amorphous graphite was also distributed in Sample 3 and induced the black color of these two samples. Like some other jades from China such as fuchsite in aventurine jade [22], graphite in nephrite [23], illite and goethite in chicken-blood stone [24], mineral inclusion is the principle color-forming factor in the two imitations. Besides, we suggest that the black color of Sample 1 was the original color of katophorite and speculate it was caused by the heterogeneous content of Fe and Mn. Even though it is easy to discriminate the real jadeite from imitations through transmission light, it is unrealistic to use in identification because once thickness exceeds 5 mm they are all lighttight.

5.2. Implications for Identification and Evaluation

Previous research reported different kinds of jadeite imitations that can be divided into 3 series: (1) artificial material such as diopside-glass [25] and synthetic jadeite [26]; (2) natural jadeite but suffering from optimizing processes such as traditional and widely known methods of bleaching, filling and dyeing as well as the new wax-permeated [27] coating [28]; and (3) natural minerals with a similar appearance, including green beryl [29], dark green amphibole and aegirine [30], green grossular jade [31], black zoisite [32] and yellow idocrase jade [33]. The natural mineral imitation is most confusing. The three fake jadeite samples in this study had a realistic appearance, crude structure and similar basic gemological characteristics such as refractive index and density. A previous study documented the analogous spectroscopic properties of pyroxene and the amphibole group, which would restrict the use of an infrared spectrometer [30]. Even though highly coincident infrared spectra are shown between pyroxene and amphibole (Figure 2a,c), they are totally different from jadeite. In addition, sometimes feldspar exhibits a similar spectrogram with jadeite (Figure A.61 in [34]). Anorthite in the present study (Sample 4) displayed the typical high-frequency region of 950–1200 cm^{-1} (Figure 2d) [35], which is convenient to distinguish it from jadeite. Therefore, we suggest infrared spectrometer is an efficient way to discriminate jadeite from its imitations. Furthermore, as the infrared spectrum of katophorite has never been reported before, its spectrogram in this study may be used as a reference in future work. In addition, we found ideal identification under XRD and propose that the 2.42 and 2.49 Å peaks of XRD can be used to discriminate black jadeite from imitations.

Even though the imitations have one or more similar characteristics, we suggest that they cannot be a potential jewelry material due to: (1) widespread outcroppings that do not meet the inherent property as “rareness” of a gem; (2) paragenesis with different proportions of dolomite that may significantly reduce its hardness and durability; and (3) the low but non-negligible concentrations of Th and U in katophorite (Sample 1) invite concern about radioactivity because of the potential harm to humans not only from their content but also their intensity. Nevertheless, we propose that they may be ideal for larger-sized ornaments on account of their moderate hardness and homogenous color. As ornaments with a fine design, they would be more affordable than natural jadeite.

However, the industrial chain of multiple imitations of black jadeite brings diagnostic challenges. Because of non-standardized equipment in different laboratories, it seems impractical to name each imitation. Otherwise, sending back such samples by reason

of miscellaneous stone is rational. In this situation, we propose that the imitation that can easily be discerned in regular testing, such as anorthite and augite, should be named. Considering that they basically conform to the national standard of jade, we recommend names such as “Hornblende jade” as Luo has reported [36]. This may provide clarity before they are put on the market.

6. Conclusions

This study integrated the techniques of FTIR, XRD, EPMA-WDS and LA-ICP-MS to examine one sample of black jadeite and three imitations so as to gain an understanding of their gemological characteristics and colorization mechanism. The real jadeite sample comprised more than 99% jadeite with trace omphacite filling in its cleavage. We suggest it be considered a new type of black jadeite as omphacite causes the black color. The imitations had different components comprising katophorite (97%), augite (66%) and anorthite (97%). They were recognized as an accessory mineral, or tinea, on the weathered crust, but dispersed graphite is documented as the source of the black color. We recommend using 2–4 sharp bands between 600 and 800 cm^{-1} of FTIR as well as the 2.42 and 2.49 Å XRD peaks to discriminate black jadeite from imitations. After cautious evaluation, we infer that the imitations do not have the potential to be jewelry due to their widespread occurrences, low hardness and unknown radioactivity from thorium and uranium.

Supplementary Materials: The following are available online at <https://www.mdpi.com/article/10.3390/cryst12050658/s1>.

Author Contributions: Conceptualization, B.Z. and K.L.; methodology, K.L. and Y.Z.; validation, B.Z. and K.L.; formal analysis, K.L. and Y.Z.; investigation, B.Z.; resources, B.Z., K.L. and Y.Z.; data curation, B.Z., K.L. and Y.Z.; writing—original draft preparation, B.Z.; writing—review and editing, B.Z.; visualization, K.L.; supervision, K.L.; project administration, B.Z.; funding acquisition, B.Z. and K.L. All authors have read and agreed to the published version of the manuscript.

Funding: This research received no external funding. The APC was funded by the authors.

Data Availability Statement: Data available on request due to restrictions on privacy. The data provided in this study can be obtained by request of the corresponding author.

Acknowledgments: Thanks to Yongjun Zhao and Shengbin Guo from Laboratory of Microscopy and Microanalysis, Wuhan Microbeam Analysis Technology Co., Ltd., Wei Gao from Wuhan SampleSolution Analytical Technology Co., Ltd., Mian Zhao from Guangzhou South Surveying & Mapping Technology Co., Ltd. and CTC Beijing Testing Technology Service Co., Ltd. for their technical guidance. We are grateful to the four reviewers and the editors for their comprehensive and valuable suggestions.

Conflicts of Interest: The authors declared that they have no conflicts of interest in this work. We declare that we do not have any commercial or associative interest that represents a conflict of interest in connection with the work submitted.

References

1. Han, C.; Wang, Y.; Liu, Y. Influence of Associated Minerals on Jadeite Naming. *J. Gems. Gemmol.* **2013**, *15*, 28–36. (In Chinese with English abstract)
2. Yin, Z. Relationships between mineralogy, petrology and gemology of “Feicui”. *Superhard Mater. Eng.* **1990**, *25*, 16–24. (In Chinese with English abstract)
3. Cheng, X.; Xiao, L. Classification and commercial evaluation of “Feicui”. *Superhard Mater. Eng.* **1990**, *25*, 8–15. (In Chinese with English abstract)
4. Zou, T.; Xia, F.; Chen, W.; Yu, X. Study on Clinopyroxene minerals of jadeite jade. *J. Gems Gemmol.* **1999**, *1*, 27–32. (In Chinese with English abstract)
5. Zhou, S.; Lai, H.; Xu, X. The prospect of black gemstones designing and processing. *J. Guilin Inst. Technol.* **2002**, *22*, 26–29. (In Chinese with English abstract)
6. Huang, D.; Xiong, W. Study on Identification and Naming of Jade Sodium Feldspathic Associated with Jade Stone. *Land Resour. Shandong Prov.* **2011**, *27*, 17–19. (In Chinese with English abstract)

7. Yang, S.; Jiang, S.; Mao, Q.; Chen, Z.; Rao, C.; Li, X.L.; Li, W.C.; Yang, W.; He, P.; Li, X. Electron Probe Microanalysis in Geosciences: Analytical Procedures and Recent Advances. *Atom Spectrosc.* **2022**, *43*, 186–200. [[CrossRef](#)]
8. Zhang, R.; Yang, S. A Mathematical Model for Determining Carbon Coating Thickness and Its Application in Electron Probe Microanalysis. *Microsc. Microanal.* **2016**, *22*, 1374–1380. [[CrossRef](#)]
9. Liu, Y.; Hu, Z.; Gao, S.; Günther, D.; Xu, J.; Gao, C.; Chen, H. In situ analysis of major and trace elements of anhydrous minerals by LA-ICP-MS without applying an internal standard. *Chem. Geol.* **2008**, *257*, 34–43. [[CrossRef](#)]
10. Ouyang, Q.; Li, H. Reviews of recent studies on black jadeite jade. *J. Gemmol.* **1999**, *26*, 417–424. (In Chinese) [[CrossRef](#)]
11. Yan, R.; Qiu, Z.; Dong, C.; Li, L. A preliminary study of typomorphic characteristics of different kinds of black jadeite jades in the world. *Acta Petrol. Mineral.* **2009**, *28*, 292–298. (In Chinese with English abstract)
12. Qiu, Z. Black jadeite. *Jewel. Sci. Technol.* **2000**, *12*, 52–53. (In Chinese)
13. Mao, J.; Chai, L.; Liu, X.; Fan, J.; Xu, J.; Jin, Z. Research of Genesis of Black Bands in Burma Jadeite. *Spectrosc. Spect. Anal.* **2013**, *33*, 2411–2415. (In Chinese with English abstract)
14. Zhang, F. Mineralogy and Gemology Study of the Black-Jadeite. Master's Thesis, China University of Geosciences, Beijing, China, 2013; pp. 1–40. (In Chinese with English abstract)
15. Guo, F. The Study on Gemological and Mineralogical of Black-Jadeite from Myanmar. Master's Thesis, Guilin University of Technology, Guilin, China, 2019; pp. 1–63. (In Chinese with English abstract)
16. He, Y.; Zu, E. Mineralogy of Burma jade from different mines. *Contrib. Geol. Miner. Resour. Res.* **2017**, *32*, 152–160. (In Chinese with English abstract)
17. Cai, S.; Zhang, E. Genesis and Formation of Amphiboles in Myanmar Raw Jadeite. *Acta Mineral. Sin.* **2018**, *38*, 50–57. (In Chinese with English abstract)
18. Zou, T.; Yu, X.; Xia, F.; Chen, W. Mineralogic components of Feicui and classification of pyroxene jade. *Yunnan Geol.* **1998**, *17*, 338–349. (In Chinese with English abstract)
19. Liu, X.; Wang, L.; Li, H.; Liu, J.; Zhao, F.; Lu, Q.; Hu, L. Systematic mineralogical classifications and nomenclatures of amphibole and pyroxene group minerals. *Acta Mineral. Sin.* **2015**, *35*, 20–28. (In Chinese with English abstract)
20. Philpotts, J.A. Redox estimation from a calculation of Eu^{2+} and Eu^{3+} concentrations in natural phases. *Earth Planet Sci. Lett.* **1970**, *9*, 257–268. [[CrossRef](#)]
21. Lv, H. *Study on Mineralogical Character of Tinea on the Weathering Crust of Feicui*; China University of Geosciences: Wuhan, China, 2008; pp. 1–59. (In Chinese with English abstract)
22. Li, Y. Gemmological Characteristic and identification of aventurine. *Superhard Mater Eng.* **1997**, *2*, 21–22. (In Chinese)
23. Han, D.; Liu, X.; Liu, Y.; Zheng, F.; Mai, A.; Zhang, H.; Wen, Z. Genesis of dolomite-related nephrite from Hetian and color-forming factors of typical nephrite in Hetian, Xinjiang. *Acta Petrol. Mineral.* **2018**, *37*, 1011–1026. (In Chinese with English abstract)
24. Guo, J.; Zhang, N.; Zhu, W.; Li, J.; Zhang, X.; Qu, J. A tentative discussion on coloration mechanism of Changhua Chicken-Blood Stone. *Acta Petrol. Mineral.* **2004**, *23*, 54–56. (In Chinese with English abstract)
25. Cai, J.; Yu, X.; Liu, C.; Yin, J. Study on Microstructure Characteristics and Crystal Chemistry of a Diopside Glass Ceramic. *J. Synth. Cryst.* **2010**, *39*, 1586–1591.
26. Li, H.; Chen, M. Experiment Study on Synthetic Jadeite Jade. *J. Gems Gemmol.* **2009**, *11*, 34–40. (In Chinese with English abstract)
27. Zhang, J.; Liu, Y.; Chen, H.; Lu, T.; Ke, J.; Zhang, Y. Experimental Study and Identification of “New Type” Wax-permeated Jadeite. *J. Gems Gemmol.* **2013**, *15*, 26–31. (In Chinese with English abstract)
28. Mu, H.; Lin, J.; Zhang, T.; Xin, C.; Li, Y. Application of Coating technology on Gemstone Optimization. *Superhard Mater. Eng.* **2020**, *32*, 59–65. (In Chinese with English abstract)
29. Zhu, H.; Liu, H.; Du, R.; Zhao, X.; Huang, Z.; Ding, X.; Chen, S. Geomological Characteristics of a Feicui Jade Imitation. *Superhard Mater. Eng.* **2020**, *32*, 59–63. (In Chinese with English abstract)
30. Li, R.; Xu, Z.; Xiong, Y.; Zhang, P.; Zhang, Y. Gemmological Characteristics of Dark Green Jadeite Imitations. *J. Gems Gemmol.* **2014**, *16*, 49–54. (In Chinese with English abstract)
31. Liu, J.; Li, R.; Xie, M.; Xu, Z. Gemmological Characteristics of Grossular Jade as Jadeite Imitation. *J. Gems Gemmol.* **2014**, *16*, 47–50. (In Chinese with English abstract)
32. Li, X.; Xu, Z.; Guo, J.; Liu, J. Zoisite Jade: One Fake Black Jadeite. *J. Gems Gemmol.* **2013**, *15*, 38–42. (In Chinese with English abstract)
33. Peng, J.; Wang, D. Preliminary Study on Idocrase Jade. *J. Gems Gemmol.* **2010**, *12*, 29–31. (In Chinese with English abstract)
34. China Association for Quality Inspection. *Gem Testing—Infrared Spectroscopy Method: T/CAQI 73-2019*; China Standard Press: Beijing, China, 2019; pp. 1–104. (In Chinese)
35. Wang, L.; Di, J. Spectroscopic Study on the Main Mineral of DuShan Yu from Henan Province, China and the Philippines. *J. Gems Gemmol.* **2021**, *23*, 39–45. (In Chinese with English abstract)
36. Luo, Y. Gemmological Characteristics of Black Hornblende Jade. *J. Gems Gemmol.* **2007**, *9*, 59–62. (In Chinese with English abstract)